# The visco-elastic multilayer program

## VEROAD

Dr. P.C. Hopman
Faculty of Civil Engineering, Delft University of Technology
NL 2600 GA Delft, The Netherlands

**The mathematical principles and derivation of a linear visco-elastic multilayer computer program are described. The mathematical derivation is based on Fourier Transformation. The program is called VEROAD, which is an acronym for Visco-Elastic ROad Analysis Delft. The program allows calculation of physical quantities like time-dependent displacements, stresses and strains, permanent deformations and dissipated energies in a multi-layer system built of visco-elastic materials. All the quantities thus depend on the velocity of the traffic, which explicitly comes into the calculations. The material model assumes the bulk modulus to be elastic and the shear modulus to be visco-elastic. The latter follows the Burgers'model.**
**For illustrative purposes, some mechanical analyses of asphaltic road structures are shown.**

*Key words*: **multilayer programs, linear visco-elastic, (permanent) deformation, stress, strain, dissipated energy.**

## 1 Introduction

The displacements, stresses and strains (dsas) in an asphaltic road structure are conventionally calculated using a linear elastic multilayer program, among which BISAR (Jong De et al. (1979) is perhaps the best known. In these programs asphalt concrete is assumed to be a linear elastic material. This assumption allows a mechanical analysis in which time dependencies (the wheelload moves) can be omitted: in (linear) elastic systems time is not a relevant parameter.

However, asphalt concrete is neither elastic nor linear. In this report it is treated as a (momentarily) linear visco-elastic material. By 'momentarily' is meant that the characteristics of the material are assumed to be constant during one passage of a wheelload. It is also assumed that the behaviour of asphalt concrete is linear. If the applied stresses are small compared to the strength at break, this assumption may be considered to be valid.
Accounting for the visco-elasticity of asphalt concrete means accounting for time dependencies, including moving of the wheel. In this study the wheel is modelled by a constant vertical load, with a circular contact area which moves with a constant velocity. Contact-effects, due to sticky surfaces, are not taken into account: both contact surfaces are considered to be smooth.

From the very start the aim was to arrive at a computer program which could be used in every-day engineering problems. Therefore preference is given to an analytical approach above an approach using finite elements. In earlier studies (Hopman (1991)), but special in the work done by Björklund (1984), the basis is laid to solve the problem under consideration. Also information from studies by Battiato et al. (1977) is used.

The general approach has four main steps:

1. 'remove' all time-dependencies of the mechanical problem by transforming all time-dependent parameters and equations to the Fourier-domain,
2. express the visco-elastic material properties in terms of frequency,
3. solve per frequency the obtained linear elastic problem (calculate dsas),
4. transform the obtained dsas inversely to the time-domain.

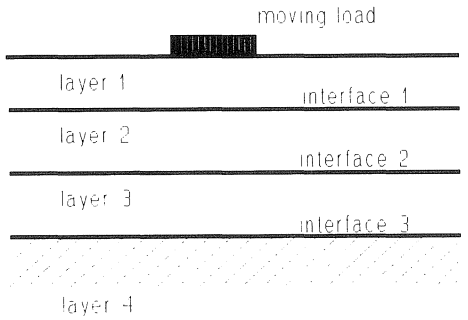


*Fig. 1. The multi-layer structure under study (for n = 4).*

The removal of the time-dependencies by Fourier transformation is well known (Björklund (1984), Ferry (1980)). In the transformed domain one has to calculate the dsas, for a number of values of the Fourier-integration variable, being the frequency. Finally, the dsas in the transformed domain must be transformed inversely to the time domain to obtain the actual dsas. This approach is known as the correspondence principle. It is assumed throughout the report that cracks do not occur, so the principle of continuity is valid. Also the principle of equilibrium is used, which states that the body remains in equilibrium. Thirdly in the consecutive equation the assumption that the material behaves visco-elastically is accounted for.
The structure under study is depicted in Figure 1. The layers are numbered downwards. The total number of layers is $n$. An interface carries the number of the layer above. The parameters which vary per layer carry a subscript referring to the layer it belongs to.

## 2 The material model

Asphaltic materials are modelled as follows:

- the bulk modulus $K$, describing the resistance to volume-changes, is linear elastic,
- the shear modulus $G$, describing the resistance to changes in shape, is linear visco-elastic.

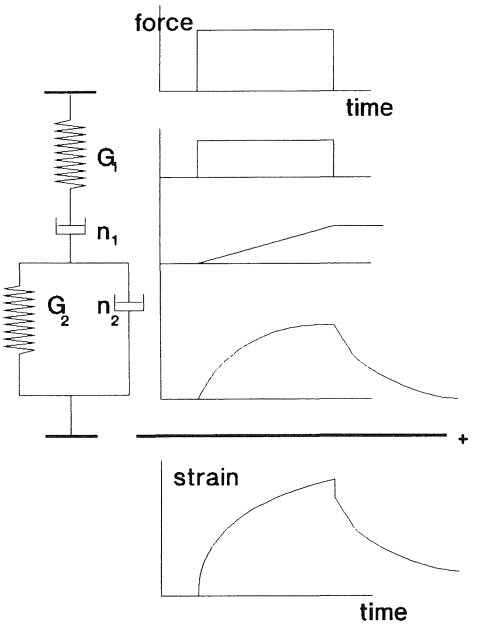


*Fig. 2. Visco-elastic model for shear modulus. Response to a square load is given.*

From a physical point of view this modelling is reasonable since well compacted asphalt mixes are elastic in compression. At the same time, asphalt mixes are rather sensitive for shear forces. This way of modelling is also used by Perloff and Moavenzadeh (1967), Ishihara (1962), Pagen (1967), Huang (1967) and others. The visco-elastic model used in this study is the Burgers' model, also known as the Maxwell-Voigt model (Figure 2).
The creep compliance $J(t)$ (inverse shear modulus), where t is the time, is:

$$J(t) = \begin{cases} 0 & t < 0 \\ \frac{1}{2}\frac{1}{G_1} & t = 0 \\ \frac{1}{G_1} + \frac{t}{\eta_1} + \frac{1}{G_2}(1 - e^{-\frac{t}{\tau_2}}) & t > 0 \end{cases} \qquad (1)$$

$$\tau_2 = \frac{\eta_2}{G_2}$$

The elastic constitutive equation are for dilatation and deviation (Timoshenko and Goodier, (1970)):

$$\sigma_v = \frac{E}{3(1-2v)}\varepsilon_v = K\varepsilon_v \qquad \tau_{ij} = \frac{E}{2(1+v)}\gamma_{ij} = G\gamma_{ij} \qquad (2)$$

where: subscript $v$ indicates volume stress or strain,
subscripts $(i,j)$ refer to the cartesian axis, $(x,y,z)$,
$E$ is Young's modulus, $\nu$ is Poisson's ratio.
$\tau$ is the shear stress, $\gamma$ is the shear strain.

The constitutive equation related to the deviational behaviour is derived here, as the one related to dilatation is similar but simpler. To simplify the notation the subscripts referring $x,y$ and $z$ are omitted. For visco-elastic materials the Boltzmann integral is used:

$$\gamma(t) = \int_{-\infty}^{t} J(t-t') \frac{\partial \tau(t')}{\partial t'} \, dt' \tag{3}$$

In the numerical implementation of equation (3) use is made of integration by parts and the lower integration limit is set to zero. Furthermore the upper limit is extended to infinite as by definition $J(t-t') = 0$, if $t - t' < 0$. One obtains (Hopman (1993)):

$$\gamma(t > 0) = \frac{1}{G_1} \tau(t) - J(t)\tau(0) + \int_{0}^{t} \tau(t-t') \frac{\partial J(t')}{\partial t'} dt' \tag{4}$$

The derivative of the compliance not necessarily vanishes if its argument becomes infinite, in which case the integral does not converge. After doing the calculations by treating the three parts individually (in accordance with the material model), one finds:

$$J^*(\omega) = \frac{1}{G_1} + \frac{1}{G_2(1+\omega^2\tau_2^2)} - i\left[\frac{1}{\omega\eta_1} + \frac{1}{G_2}\frac{\omega\tau_2}{1+\omega^2\tau_2^2}\right] = J^*_r + iJ^*_i \tag{5}$$

where the real and imaginary parts of the shear compliance are defined (note the subscripts, $i$ is the imaginary unit). For very small $\omega$:

$$J^*_r = \frac{1}{G_1} + \frac{1}{G_2} \qquad J^*_i = \frac{-1}{\omega\eta_1} \tag{6}$$

Obviously the imaginary part is not defined for $\omega = 0$. This essentially means that static loads are not allowed in these calculations, as will become evident later on.
Having the creep and bulk compliancies in frequency domain, the Poisson's ratio can be obtained by using the basic mutual equations between the mechanical parameters $K$ (bulk modulus), $G$ (shear modulus), $E$ (Young's modulus) and $\nu$ (Poisson's ratio).

$$\begin{aligned} \nu^*(\omega) &= \frac{3J^*(\omega) - 2\chi^*}{2(3J^*(\omega) + \chi^*)} \\ &= \frac{9J^{*2}_r - 2\chi_0^2 - 3J^*_r\chi_0 + 9J^{*2}_i}{2(3J^*_r + \chi_0)^2 + 18J^{*2}_i} + i\frac{9J^*_i\chi_0}{2(3J^*_r + \chi_0)^2 + 18J^{*2}_i} \\ &= \nu^*_r(\omega) + i\nu^*_i(\omega) \end{aligned} \tag{7}$$

where $\nu^*_r$ and $\nu^*_i$ are defined and $\chi_0$ is the bulk compliance. For very small $\omega$:

$$\nu^*_r = 0.5 \qquad \nu^*_i = -\frac{1}{2}\chi_0\eta_1\omega \tag{8}$$

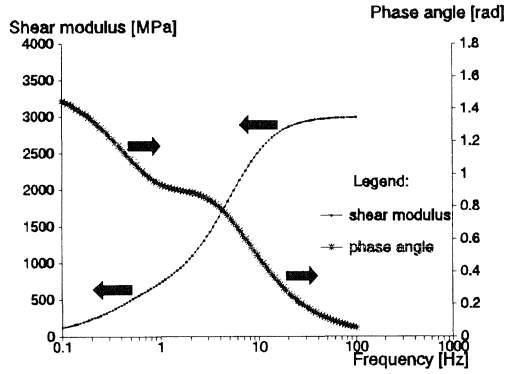


*Fig. 3a. Shear modulus and phase angles versus frequency.*

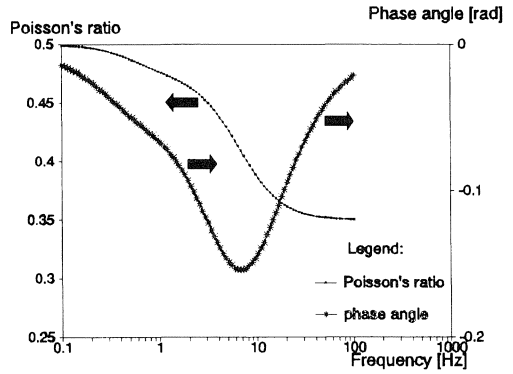


*Fig. 3b. Poisson's ratio and phase angle versus frequency.*

In Figures 3a/b the frequency dependency of the mechanical parameters and their phase angles is given. The values of the parameters in Burgers'model were: $G_1 = 3000$ MPa, $G_2 = 1500$ MPa, $\eta_1 = 200$ MPa.s, $\eta_2 = 150$ MPa.s and $K = 9000$ MPa. The given equations are valid for a sample temperature of some 25°C. The stress signal which occurs in the road contains frequencies between 0.1 and 50 Hz (depending primarily on the velocity of the traffic). Thus, from Figures 3 it is clear that one is obliged to account for the visco-elastic properties of the material.

## 3 Fourier transformation of the moving circular load

The wheel load is assumed to have a circular contactarea and to slide over the surface ($z = 0$), with a constant velocity along the $x$-axis. The coordinate system ($x,y,z$) is fixed unto the construction, where z is perpendicular into the construction. To the axis of the load the Cartesian coordinate system ($u, y', z'$) is fixed. The parameter $u$ equals $x$ for $t = 0$, then decreases and becomes negative

at the moment that the axis of the load is above the point of consideration. Both coordinate systems are interrelated by:

$$u = x - v.t \qquad y' = y \qquad z' = z \tag{9}$$

The load is zero outside the contact area. Thus, if $y \leq a$ the load is:

$$\sigma_z(x, y, z = 0, t) = -\sigma_0 \left\{ H(x - vt - \sqrt{a^2 - y^2}) - H(x - vt + \sqrt{a^2 - y^2}) \right\} \tag{10}$$

where $H(t)$ is the Heaviside function,
$v$ is the velocity in $x$-direction (m/s),
a is the radius of the contact area (m),
$\sigma_0$ is the vertical contact stress (MPa).

The vertical load can thus be written as:

$$\sigma_z(u, y, 0, t) = -\sigma_0 H(r - a) \qquad (r^2 = x^2 + y^2) \tag{11}$$

The load can be written as a Hankel-transformation:

$$\sigma_z(u, y, 0, t) = -\sigma_0 a \int_0^\infty J_1(\rho a) J_0(\rho r) \mathrm{d}\rho \tag{12}$$

where $J_0$ and $J_1$ are the zero-th and first order Bessel function.

This integral-representation may be linked to a two-dimensional Fourier-transformation, as is shown more strictly elsewhere. One obtains:

$$\sigma_z(u, y, 0, t) = -\sigma_0 a \frac{1}{2\pi} \int_{-\infty}^{\infty} \int_{-\infty}^{\infty} \frac{1}{\rho} J_1(\rho a) e^{-i(\zeta u + \xi y)} \mathrm{d}\zeta \mathrm{d}\xi \qquad (\rho^2 = \zeta^2 + \xi^2) \tag{13}$$

Fourier transformation with respect to time and using the identity:

$$\int_{-\infty}^{\infty} e^{-i\alpha x} \mathrm{d}x = 2\pi\delta(a) \tag{14}$$

in which $\delta$ indicates the Kronecker delta-function yields ($y \leq a$):

$$\begin{aligned} \tilde{\sigma}_z &= \frac{-\sigma_0 a}{v\sqrt{2\pi}} e^{-i\frac{\omega x}{v}} \int_{-\infty}^{\infty} \frac{1}{\lambda} J_1(\lambda a) e^{-i\xi y} \mathrm{d}\xi \\ &= \frac{-2v\sigma_0}{\omega} \sqrt{\frac{2}{\pi}} e^{-i\frac{\omega x}{v}} \sin\left(\frac{\omega}{v}\sqrt{a^2 - y^2}\right) \qquad \left(\lambda^2 = \frac{\omega^2}{v^2} + \xi^2\right) \end{aligned} \tag{15}$$

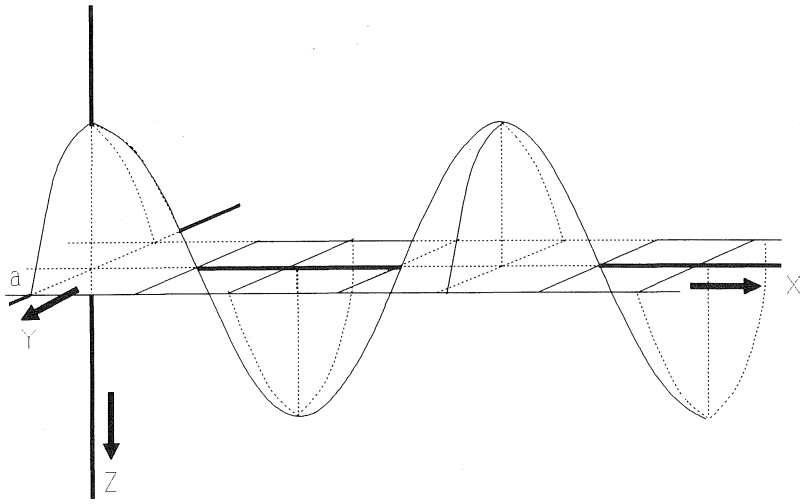


*Fig. 4. Typical example of the real part of the load in Fourier-domain.*

It is required that the velocity does not equal zero. This is physically understood by recalling that a static load will fall through the construction due to the dashpot $\eta_1$ in the Burgers' model. The real part of equation (15) is shown graphically in Figure 4. The load in frequency domain has the following characteristics:

- the period along the $x$-axis depends on the velocity of the wheel in the time domain,
- the period along the $y$-axis depends on this velocity also,
- both periodicities depend on the Fourier parameter $\omega$,
- no axial symmetry,
- the radius of the circular load limits the range on the $y$-axis.

The shape of the load is sinusoidal in both directions. One may look upon it as a (co)sinusoidally disformed cylinder. The wavelength of the 'deformation' depends, among others, on the angular frequency $\omega$; both in the direction of the $x$-axis and in the direction of the $y$-axis. The Fourier transform of an (optionally) applied shear load ($\tau_{xz}$ or $\tau_{yz}$ at $z = 0$) can be obtained analogously.

## 4 Dsas in Fourier domain

To determine the displacements, stresses and strains (dsas) in Fourier domain the correspondence principle is used. For each frequency a linear elastic calculation is carried out, using the load obtained above and the material characteristics given in equations (5) and (7). Essentially we follow the Burmister approach (Burmister, 1945). Mathematical aspects are taken from the work of Van Cauwelaert (1988), who calculated dsas in linear elastic multilayer system for non-symmetric loads in a Cartesian coordinate system. The starting point are the elastic, equilibrium and continuity requirements. Airy suggested to assume that potential or stress functions exist, from which the dsas can be derived. In Cartesian coordinates the stresses are given by:

$$\tilde{\sigma}_x = \frac{\partial}{\partial z}(\upsilon^*\nabla^2\phi - \frac{\partial^2\phi}{\partial x^2}) + \frac{\partial^2\psi}{\partial x\partial y} \qquad \tilde{\sigma}_y = \frac{\partial}{\partial z}(\nu^*\nabla^2\phi - \frac{\partial^2\phi}{\partial y^2}) - \frac{\partial^2\psi}{\partial x\partial y}$$

$$\tilde{\sigma}_z = \frac{\partial}{\partial z}\left[(2-\upsilon^*)\nabla^2\phi - \frac{\partial^2\phi}{\partial z^2}\right] \qquad \tilde{\tau}_{yz} = \frac{\partial}{\partial y}\left[(1-\nu^*)\nabla^2\phi - \frac{\partial^2\phi}{\partial z^2}\right] - \frac{1}{2}\frac{\partial^2\psi}{\partial x\partial z}$$

$$\tilde{\tau}_{xz} = \frac{\partial}{\partial x}\left[(1-\nu^*)\nabla^2\phi - \frac{\partial^2\phi}{\partial z^2}\right] + \frac{1}{2}\frac{\partial^2\psi}{\partial y\partial z} \qquad \tilde{\tau}_{xy} = \frac{\partial^3\phi}{\partial x\partial y\partial z} - \frac{1}{2}(\frac{\partial^2\psi}{\partial x^2} - \frac{\partial^2\psi}{\partial y^2}) \qquad (16)$$

in which:

$$\nabla^2\phi - \frac{\partial^2\phi}{\partial x^2} + \frac{\partial^2\phi}{\partial y^2} + \frac{\partial^2\phi}{\partial z^2} \qquad (17)$$

The functions $\phi$, $\psi$, $f$ and $g$ are defined in the frequency domain. As they do not play a role in the time domain, they do not carry a tilde. The equilibrium condition is fulfilled if the potential functions $\phi$ and $\psi$ are solutions of the double, respectively single Laplacian:

$$\nabla^2\nabla^2\phi = 0 \qquad \nabla^2\psi = 0 \qquad (18)$$

The displacements can be obtained from the stress functions by:

$$\tilde{u}_x = -\frac{1}{2}J^*(\frac{\partial^2\phi}{\partial x\partial z} - \frac{\partial\psi}{\partial y}) \qquad \tilde{u}_y = -\frac{1}{2}J^*(\frac{\partial^2\phi}{\partial y\partial z} + \frac{\partial\psi}{\partial x}) \qquad \tilde{u}_z = \frac{1}{2}J^*\left[2(1-\upsilon^*)\nabla^2\phi - \frac{\partial^2\phi}{\partial z^2}\right] \qquad (19)$$

They are related with the strains by:

$$\tilde{u}_x = \int \tilde{\epsilon}_x \,\mathrm{d}x \qquad \tilde{u}_y = \int \tilde{\epsilon}_y \,\mathrm{d}y \qquad \tilde{u}_z = \int \tilde{\epsilon}_z \,dz \qquad (20)$$

It is derived by Hopman (1994) that the following equations hold for the stress functions:

$$\phi = \frac{a}{\upsilon\sqrt{2\pi}} e^{-i\frac{\omega x}{\upsilon}} \int_{-\infty}^{\infty} \frac{J_1(\lambda a)}{\lambda} e^{-i\xi y} f(z,\lambda)\mathrm{d}\xi \qquad \psi = \frac{-2a}{\upsilon^2\sqrt{2\pi}} e^{-i\frac{\omega x}{\upsilon}} \int_{-\infty}^{\infty} \frac{\omega}{\xi}\frac{J_1(\lambda a)}{\lambda} e^{-i\xi y} g(z,\lambda)\mathrm{d}\xi \qquad (21)$$

with:

$$f(z,\lambda) = f(z) = Ae^{\lambda z} - Be^{-\lambda z} + Cze^{\lambda z} - zDe^{-\lambda z} \qquad g(z,\lambda) = Pe^{\lambda z} - Qe^{-\lambda z} \qquad (22)$$

In equations 21 and 22 one recognizes the Burmister approach. The problem is now to determine the parameters $A$, $B$, $C$, $D$, $P$ and $Q$ for each layer such, that the appropriate boundary conditions are fulfilled.
At the top of the construction the boundary condition due to the load ($\sigma_z$) is:

$$A_1\lambda^3 + B_1\lambda^3 - (1 - 2\nu_1^*)\, C_1\lambda^2 + (1 - 2\nu_1^*)\, D_1\lambda^2 = \sigma_0 \tag{23}$$

whereas at the surface shear stresses might be applied (under the load):

$$\tilde{\tau}_{yz} = \tau_1 \qquad \tilde{\tau}_{xz} = \tau_2 \tag{24}$$

Thus, again after lengthy calculation:

$$\lambda^2 A_1 - \lambda^2 B_1 + 2\nu_1^* \lambda C_1 + 2\nu_1^* - \frac{\omega^2}{v^2}\frac{1}{\xi^2}\lambda P_1 - \frac{\omega^2}{v^2}\frac{1}{\xi^2}\lambda Q_1 = i\frac{1}{\xi}\tau_1$$
$$\lambda^2 A_1 - \lambda^2 B_1 + 2\nu_1^* \lambda C_1 + 2\nu_1^* \lambda D_1 + \lambda P_1 + \lambda Q_1 = i\frac{v}{\omega}\tau_2 \tag{25}$$

As the physical quantities must be zero at infinite depth, the coefficients of $e^{\lambda z}$ must be zero. Thus:

$$A_n = C_n = P_n = 0 \tag{26}$$

These conditions together yield six equations to determine the six unknowns. In case the structure is a halfspace ($n = 1$), the parameters can be solved analytically. One may write equations (23 and 25) as:

$$M_{01}(A_1 B_1 C_1 D_1 P_1 Q_1)^T = (1\ 0\ 0)^T \tag{27}$$

in which $M_{01}$ indicates the matrix set up by these equations and the superscript $T$ indicates that the matrix is transposed. In case a multilayer system is to be analyzed extra conditions apply. The vertical stress $\sigma_z$, the vertical displacement $u_z$ and the shear stresses $\tau_{yz}$ and $\tau_{xz}$ are equal at both sides of the interface $j$. Thus:

$$\tilde{\sigma}_{z_j} = \tilde{\sigma}_{z_{j+1}} \qquad \tilde{u}_{z_j} = \tilde{u}_{z_{j+1}} \qquad \tilde{\tau}_{xz_j} = \tilde{\tau}_{xz_{j+1}} \qquad \tilde{\tau}_{yz_j} = \tilde{\tau}_{yz_{j+1}} \tag{28}$$

Furthermore certain conditions should be fulfilled with respect to the horizontal displacements. Two cases are distinguished:

– full friction or full adhesion, meaning that no slip occurs between the two layers:

$$\tilde{u}_{x_j} = \tilde{u}_{x_{j+1}} \qquad \tilde{u}_{x_j} = \tilde{u}_{x_{j+1}} \tag{29}$$

– no friction or no adhesion, which is equivalent to the observation that shear stresses cannot exist over the interface. Thus:

$$\tilde{\tau}_{yz_j} = \tilde{\tau}_{yz_{j+1}} = 0 \qquad \tilde{\tau}_{xz_j} = \tilde{\tau}_{xz_{j+1}} = 0 \tag{30}$$

So for each interface six equations are obtained to determine the six parameters of the stress functions. In literature (De Jong et al. (1978), van Cauwelaert (1988)) intermediate stages between

the two extremes are proposed. In this study these intermediate conditions are not discussed.

These conditions enable calculation of the stress functions, and thus of the dsas, in frequency or Fourier, domain. Obviously one has to deal with matrices to determine all the unknowns. An exact and numerically very fast route to do so has been described by van Cauwelaert (1992). Its application to VEROAD is given by Hopman (1994).
Combining the boundary conditions one may obtain the parameters for a higher layer (layer p) from those of a lower layer (layer p + 1) by:

$$(A_p\ B_p\ C_p\ D_p\ P_p\ Q_p\ )^T = M_{pp}^{-1}\ M_{p\,p+1}\ (A_{p+1}\ B_{p+1}\ C_{p+1}\ D_{p+1}\ P_{p+1}\ Q_{p+1})^T \tag{31}$$

The complete solution of the system for a *n*-layer structure is obtained by iteration, finally leading to the boundary conditions at the surface (equation 27). It is given by:

$$M_{01}^{-1}\ [M_{11} \cdot M_{22}^{-1}\ M_{23} \cdot \ldots \cdot M_{n-1\,n-1}^{-1}\ M_{n-1\,n}\ (0\ B_n\ 0\ D_n\ 0\ Q_n\ )^T] = (1\ 0\ 0)^T \tag{32}$$

Thus the coefficients $B_n$, $D_n$ and $Q_n$ can be calculated by solving this system. The coefficients for the other layers can be calculated subsequently using equation (31). The matrix product at each interface shows that the coefficients *P* and Q are independent from *A*, *B*, *C* and *D*. Thus, if only a vertical load is applied, *P* and *Q* are zero for all layers.
It is remarked here that the presence of the positive exponentials in the matrix (from equation 22) can lead to numerical errors if $z \to \infty$ and / or $\lambda \to \infty$. To prevent these errors advantage is taken from the fact that in each row the same exponent occurs. The exponentials are isolated by writing

$$M_{pq}^{-1} = M'_{pq1}\ e^{-\lambda z_p} + M'_{pq2}\ e^{\lambda z_p} \tag{33}$$

The elements in $M'_{pq1}$ and $M'_{pq2}$ are defined by comparing them with those of $M_{pp}^{-1}$. The apostrophes are to remember that the original matrix is an inverse matrix. It appears that both $M'_{pq1}$ and $M'_{pq2}$ contain rows with solely zero-valued elements. The same holds, mutatis mutandi, for matrix $M_{p\,p+1}$, where the columns contain zero-valued elements.

$$M_{p\,p+1} = M_{p\,p+1\,1} e^{\lambda z_p} + M_{p\,p+1\,2} e^{-\lambda z_p} \tag{34}$$

The matrix-products in (31) or (32) are:

$$M_{pp}^{-1}\ M_{p\,p+1} = [M'_{pp\,1} e^{-\lambda z_p} + M'_{pp\,2} e^{-\lambda z_p}]\ [M_{p\,p+1\,1} e^{-\lambda z_p} + M'_{p\,p+1\,2} e^{-\lambda z_p}] \tag{35}$$

It is observed that the products of the matrices contain much zero-valued elements. The non-zero elements in these matrices are listed below and new names are given to the (3*3) matrices (containing the elements of the matrix product indicated):

$$
\begin{aligned}
&M'_{pp1}\,M_{p\,p+1\,1}\text{: (1,1) (1,3) (1,5) (3,1) (3,3) (3,5) (5,1) (5,3) (5,5): } MA_p\\
&M'_{pp1}\,M_{p\,p+1\,2}\text{: (1,2) (1,4) (1,6) (3,2) (3,4) (3,6) (5,2) (5,4) (5,6): } MB_p\\
&M'_{pp2}\,M_{p\,p+1\,1}\text{: (2,1) (2,3) (2,5) (4,1) (4,3) (4,5) (6,1) (6,3) (6,5): } MC_p\\
&M'_{pp2}\,M_{p\,p+1\,2}\text{: (2,2) (2,4) (2,6) (4,2) (4,4) (4,6) (6,2) (6,4) (6,6): } MA_p
\end{aligned}
\tag{36}
$$

These new matrices contain also zero-valued elements. The recognition of this, and especial with respect to the positions of these elements, is important for the numerical implementation. It is noted that special multiplication rules exist. The equations below indicate that the positions of the zero-valued elements of the product of two new matrices are identical to one of them.

$$
\begin{aligned}
&MA \cdot MB = MB \qquad MB \cdot MD = MB\\
&MC \cdot MB = MD \qquad MD \cdot MD = MD
\end{aligned}
\tag{37}
$$

Equation (32) can be now be written as:

$$
\begin{aligned}
(A_pB_pC_pD_pP_pQ_p)^T = [MA_p + MB_pe^{-2\lambda z_p} + MC_pe^{2\lambda z_p} + MD_p] *\\
* (A_{p+1}\,B_{p+1}\,C_{p+1}\,D_{p+1}\,P_{p+1}\,Q_{p+1})^T
\end{aligned}
\tag{38}
$$

Thanks to the ordering of the zero-valued elements one can split this and write it as a set of equations:

$$
\begin{cases}
(A_p0C_p0P_p0)^T = MA_p(A_{p+1}0C_{p+1}0P_{p+1}0)^T + MB_p(0B_{p+1}0D_{p+1}0Q_{p+1})^Te^{-2\lambda z_p}\\
(0B_p0D_p0Q)^T = MC_p(A_{p+1}0C_{p+1}0P_{p+1}0)^Te^{-2\lambda z_p} + MD_p(0B_{p+1}0D_{p+1}0Q_{p+1})^T
\end{cases}
\tag{39}
$$

Thus the 6*6 matrices are written as 3*3 matrices:

$$
\begin{cases}
(A_pC_pP_pQ_p)^T = MA_p(A_{p+1}C_{p+1}P_{p+1})^T + MB_p(B_{p+1}D_{p+1}Q_{p+1})^Te^{-2\lambda z_p}\\
(B_pD_pQ_p)^T = MC_p(A_{p+1}C_{p+1}P_{p+1})^Te^{-2\lambda z_p} + MD_p(B_{p+1}D_{p+1}Q_{p+1})^T
\end{cases}
\tag{40}
$$

The system can be solved by subsequent substitution. Starting with the lowest interface (and writing the exponential explicitly) we have ($A_n = C_n = Q_n = 0$):

$$
\begin{aligned}
&(A_{n-1}C_{n-1}P_{n-1})^T = MB_{n-1}\,(B_nD_nQ_n)^Te^{-2\lambda z_{n-1}}\\
&(B_{n-1}D_{n-1}Q_{n-1})^T = MD_{n-1}\,(B_nD_nQ_n)^T
\end{aligned}
\tag{41}
$$

This is substituted in the equation for interface $p = n - 2$, the one lowest, given by (40).

$$
\begin{aligned}
(A_{n-2}C_{n-2}P_{n-2})^T &= MA_{n-2}\,(A_{n-1}C_{n-1}P_{n-1})^T + MB_{n-2}\,(B_{n-1}D_{n-1}Q_{n-1})^T e^{-2\lambda z_{n-2}} \\
&= [MA_{n-2}\,MB_{n-1}\,e^{-2\lambda z_{n-1}} + MB_{n-2}MD_{n-1}\,e^{-2\lambda z_{n-2}}]\,(B_nD_nQ_n)^T \\
&= e^{-2\lambda z_{n-2}}\,MB_{n-2\,n-1}\,(B_nD_nQ_n)^T \\
(B_{n-2}D_{n-2}Q_{n-2})^T &= MC_{n-2}\,(A_{n-1}C_{n-1}P_{n-1})^T e^{2\lambda z_{n-2}} + MD_{n-2}\,(B_{n-1}D_{n-1}Q_{n-1})^T \\
&= [MC_{n-2}\,MB_{n-1}\,e^{-2\lambda(z_{n-1}-z_{n-2})} + MB_{n-2}MD_{n-1}]\,(B_nD_nQ_n)^T \\
&= MD_{n-2\,n-1}\,(B_nD_nQ_n)^T
\end{aligned}
\tag{42}
$$

where the two following definitions hold:

$$
\begin{aligned}
MB_{n-2\,n-1} &= MA_{n-2}\,MB_{n-1}\,e^{-2\lambda(z_{n-1}-z_{n-2})} + MB_{n-2}MD_{n-1} \\
MD_{n-2\,n-1} &= MC_{n-2}\,MB_{n-1}\,e^{-2\lambda(z_{n-1}-z_{n-2})} + MD_{n-2}MD_{n-1}
\end{aligned}
\tag{43}
$$

Here $z_{n-1} - z_{n-2}$ is the thickness of the one lowest layer (layer $n$–1) and is always >0. The exponent vanishes for larger $\lambda$. This is done successively for all interfaces, resulting in:

$$
\begin{aligned}
(A_1C_1P_1)^T &= e^{-2\lambda z_1}\,MB_{12\ldots n-2\,n-1}\,(B_nD_nQ_n)^T \\
(B_1D_1Q_1)^T &= \qquad MB_{12\ldots n-2\,n-1}\,(B_nD_nQ_n)^T
\end{aligned}
\tag{44}
$$

To solve the system for $B_n$, $D_n$ and $Q_n$ this is rewritten as a set of six equations in which $a_{1j} = MB_{1j}$, $a_{3j} = MB_{2j}$, $a_{5j} = MB_{3j}$, $a_{2j} = MD_{1j}$, $a_{4j} = MD_{2j}$ and $a_{6j} = MD_{3j}$:

$$
\begin{aligned}
A_1 &= a_{11}B_n + a_{12}D_n + a_{13}Q_n \\
B_1 &= a_{21}B_n + a_{22}D_n + a_{23}Q_n \\
C_1 &= a_{31}B_n + a_{32}D_n + a_{33}Q_n \\
D_1 &= a_{41}B_n + a_{42}D_n + a_{43}Q_n \\
P_1 &= a_{51}B_n + a_{52}D_n + a_{53}Q_n \\
Q_1 &= a_{61}B_n + a_{62}D_n + a_{63}Q_n
\end{aligned}
\tag{45}
$$

The six parameters $a_{mj}$ are inserted in the surface conditions (32) to obtain a set of 3 equations with three unknowns ($B_n$, $D_n$, $Q_n$). This system can easily be solved. Finally, the convergence over the variable $\lambda$ is ensured as is seen from equation (42): they all contain exponentials with finite values of the depth z. With one exception: the determination of ($B_1$, $D_1$, $Q_1$). This means that for $z = 0$ a convergence problem may occur. To prevent this it is proposed by Van Cauwelaert (1992) to calculate these coefficients directly from the three surface conditions.

## 5 Dsas in time domain

Now the displacements, stresses and strains (dsas) have been determined in the Fourier or frequency domain. To get them in the time domain, they have to be inversely Fourier transformed, according to:

$$\mathrm{dsas}(t) = \frac{1}{\sqrt{2\pi}} \int_{-\infty}^{+\infty} \tilde{\mathrm{dsas}}(\omega) e^{i\omega t} \mathrm{d}\omega \tag{46}$$

## 6 Validation of VEROAD

Veroad has been validated by comparing the longitudinal and transversal strains as obtained in full scale tests with those calculated. In such full scale tests an actual truck wheel rides over an actual asphaltic structure. The measurements and calculations refer to a three layer asphaltic structure, which has been studied extensively in the LINTRACK, which is a full scale test facility at the Delft University of Technology (Groenendijk et al. (1994). The asphaltic structure and the load conditions are given in table 1. The visco-elastic material properties have been determined using a four point bending test (Sassen (1991)).

Measurements of the longitudinal and transversal strains with LINTRACK are reported by Groenendijk et al. [9] and reported in Figures 5a and 5b. These figures include the strains calculated using VEROAD. The measured strains are obtained at the bottom of the asphalt layer. The figures should be read as follows: The strain in the gauge depends on the longitudinal distance to the wheel (the transversal distance is zero ($y = 0$)). When the wheel is right above the gauge, the strains are not yet maximum. That will be the case when the wheel has passed the gauge. The strain curves are asymmetric in time, indicating visco-elastic effects. Thus these measurements cannot be modelled with linear elastic multilayer programs. VEROAD gives good results as the time retardation effects are within the material model.

Table 1. Loading, pavement and material characteristics.

| | | | | | |
|---|---|---|---|---|---|
| Wheel load | : 75 kN | | Velocity | : 5.5 m/s | |
| Contact pressure | : 0.70 MPa | | Temperature | : 23°C | |
| Radius of contact area | : 158.5 mm | | Type of wheel | : 425/65 R22.5 | |
| layer thickness | $\eta_1$ [MPa.s] | $\eta_2$ [MPa.s] | $G_1$ [MPa] | $G_2$ [MPa] | $K$ [MPa] |
| 148 mm | 138 | 71 | 3200 | 2837 | 9000 |
| ∞ | ∞ | ∞ | 60 | ∞ | 180 |

A good fit between the measured and calculated values of the longitudinal as well as the transversal signal is obtained. The time retardation effects are clearly seen in both calculated strain curves: as the maximum in both curves only develops when the wheel has passed.

The longitudinal strain curve shows compression first, then tension and thereafter compression again. After the load passage the longitudinal strain will always be zero (no permanent deformation). The transversal strain curve has no compression, only tension that decreases slowly to a permanent rest. Even better fits, especially with respect to the second minimum in the longitudinal strain can be obtained if some 15 cm of the sand under the asphalt is given some visco-elasticity. This effect is more pronounced in cases were thinner pavement structures are studied (Nilsson et al. (1996)).

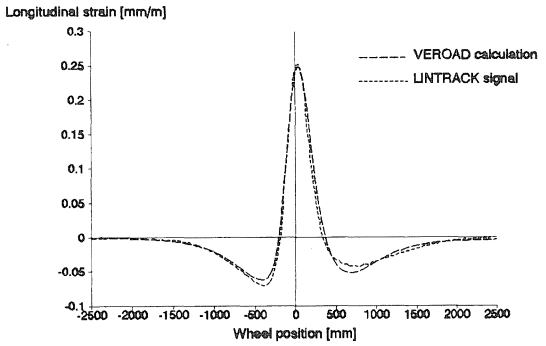


*Fig. 5a. Measured and calculated longitudinal strains.*

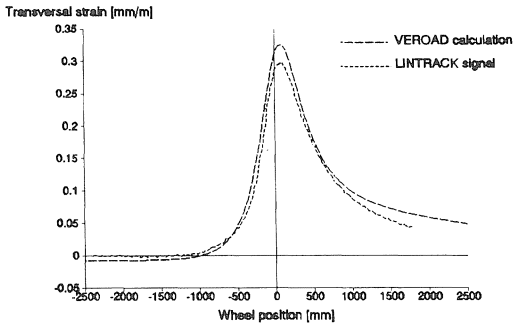


*Fig. 5b. Measured and calculated transversal strains.*

It is also noted here that the maximum of the longitudinal strain is smaller than the maximum of the transversal strain. This will not be found using elastic programs, but in the visco-elastic program presented here it is natural consequence of the fact that the load moves. This is a kind of anisotropy in the loading, and thus in the resulting strains. This notation is very important if a road design system is based on the maximum horizontal strain at the bottom of the asphalt layer.

# 7 Some results

## 7.1 *Stresses and strains*

Stresses and strains have been calculated for a 3-layer structure built from materials characterised in table 2. The characteristics of the load are: velocity: 5 m/s, radius of contact area: 150 mm, contact stress: 0.707 MPa (wheelload $50*10^3$N).

In Figure 6 the calculated longitudinal and transversal stresses and strains at the bottom of the asphaltic layer at a depth of 400 mm is shown, versus the longitudinal distance to the wheel (at $t = 0$). The load moves from left to right. At the moment the load is at $x = 0$, a snapshot is taken of the longitudinal stress and strain distribution. The time retardation can be read from the maximum in

Table 2. Construction and Material Properties.

| layer | thickness (mm) | $G_1$ (MPa) | $G_2$ (MPa) | $\eta_1$ (MPa.s) | $\eta_2$ (MPa.s) | $K$ (MPa) |
|---|---|---|---|---|---|---|
| 1 | 100 | 3000 | 1500 | 200 | 150 | 9000 |
| 2 | 300 | 4000 | 5000 | 500 | 1000 | 20000 |
| 3 | ∞ | 37 | ∞ | ∞ | ∞ | 112 |

both the strain curves, which is behind the wheel. This time retardation can be much more outspoken. It depends strongly on the material parameters and the velocity of the load. It is noted that time retardation is very evident in the longitudinal and vertical displacements.

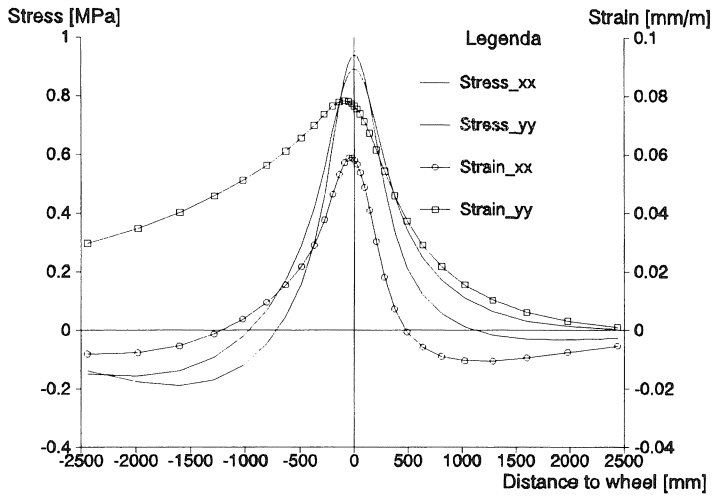


*Fig. 6. Stresses and strains at the bottom of the asphaltic layer (+: tension, –: compression).*

## 7.2 *The permanent dsas*

The permanent displacements, stresses and strains (dsas($t \to \infty$)) can be obtained directly from theory (Björklund (1984), Battiato et al. (1977), Hopman (1994)). The dsas(t) can be obtained from the Fourier domain by inverse transformation, as indicated in equation (46).
Differentiating to time t yields:

$$\frac{\partial}{\partial t}\,\mathrm{dsas}(t) = \frac{1}{\sqrt{2\pi}} \int_{-\infty}^{\infty} i\omega \;\; \tilde{\mathrm{dsas}} \;\; e^{i\omega t}\,\mathrm{d}\omega \tag{47}$$

and by inverting

$$\frac{1}{\sqrt{2\pi}} \int_{-\infty}^{\infty} \frac{\partial}{\partial t}\,\mathrm{dsas}(t)\; e^{i\omega t}\,\mathrm{d}t \;=\; i\omega \;\; \tilde{\mathrm{dsas}}(\omega) \tag{48}$$

Recognize that by definition dsas(-∞) = 0. Thus the permanent part of dsas is:

$$\int_{-\infty}^{\infty} \frac{\partial}{\partial t}\,\mathrm{dsas}(t)\;\mathrm{d}t \;=\; \int_{-\infty}^{\infty} d(\mathrm{dsas}(t)) \;=\; \mathrm{dsas}(\infty) - \mathrm{dsas}(-\infty) \;=\; \mathrm{dsas}(\infty) \tag{49}$$

If in (48) $\omega \to 0$, the permanent part of dsas(t) is obtained:

$$\mathrm{dsas}_p \;=\; \lim_{\omega \to 0} \sqrt{2\pi}\, i\omega\, \tilde{\mathrm{dsas}}(\omega) \tag{50}$$

It is noted that, thanks to $\omega$ in the numerator, the singularity in the shear modulus for $\omega = 0$, is prevented.

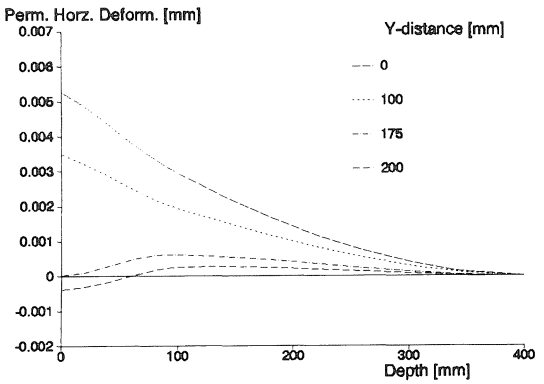


*Fig. 7a. Permanent vertical deformation versus depth at various lateral distances.*

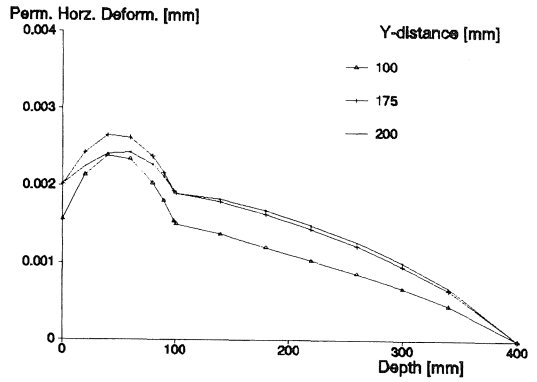


*Fig. 7b. Permanent horizontal deformation.*

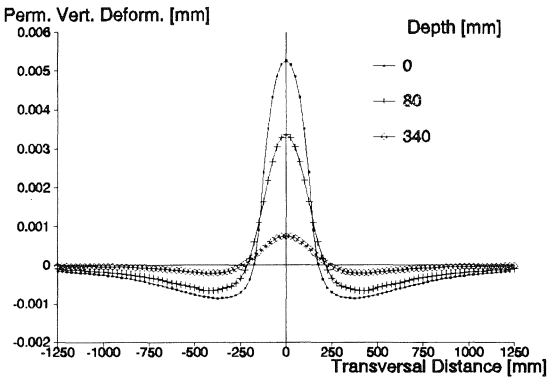


*Fig. 8a. Permanent vertical deformation versus lateral distance at several depths.*

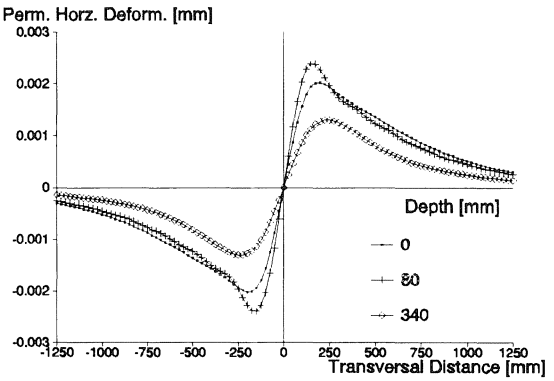


*Fig. 8b. Permanent horizontal displacement.*

In figures 7a/b the vertical ($u_z$) and horizontal ($u_y$) permanent deformations are given as they occur after one single load (for a full Burgers'model). The net displacement of a volume-element at a ($y$,$z$)-position is the square root of the quadratic sum of both. There is no permanent deformation in the $x$-direction, as follows directly from theory. To obtain the shape of permanent deformations as they occur in the road one has to superimpose these curves in accordance with the loads and the lateral wander. In Figures 8a/b the vertical and horizontal deformations per depth are given. One recognizes the width of the tyre. Of course there is (anti-) symmetry. Interesting is that the maximum horizontal deformation is at a depth of about 80 mm.

## 7.3 *Energy Dissipation*

In general, the energy put in a construction by a transient load, has two parts: the elastic (recoverable) and inelastic (irrecoverable, dissipated). The first one is elastic. The second one not: it is converted into heat or it changes the material somewhat. These changes amount to damage (crack growth). The inelastic, dissipated energy is of interest here. The energy, dissipated by a moving wheel in a volume-element at ($x_0$, $y_0$, $z_0$), is given by:

$$W_{dis} = \int_{-\infty}^{\infty} \left[ \sigma_{xx}\dot{\varepsilon}_{xx} + \sigma_{yy}\dot{\varepsilon}_{yy} + \sigma_{zz}\dot{\varepsilon}_{zz} + \sigma_{xy}\dot{\varepsilon}_{xy} + \sigma_{xz}\dot{\varepsilon}_{xz} + \sigma_{yz}\dot{\varepsilon}_{yz} \right] dt$$

The time elapse involved is the time it takes the wheelload to come from far (minus infinity) and to go to far (plus infinity). One should note that extra-ordinary results are obtained if the energy is analyzed term by term. Due to the rotation of the principal axis during passage of the wheel such an analysis is not physically justified. Nevertheless, for the sake of explanation the 'horizontal-energy-terms' are considered in Figures 9a/b. The longitudinal stresses and strains, also presented in Figure 6, are plotted in mutual dependence (Lissajou-plot). The areas enclosed equal the dissipated energy terms. On passage of a wheel, for both the longitudinal and transversal signals, first the upper branch is taken up to the maximum. Subsequently the lower branch is followed (so the path is clockwise). The curve is not closed as some permanent deformation exists in the construction after passage of a wheel.

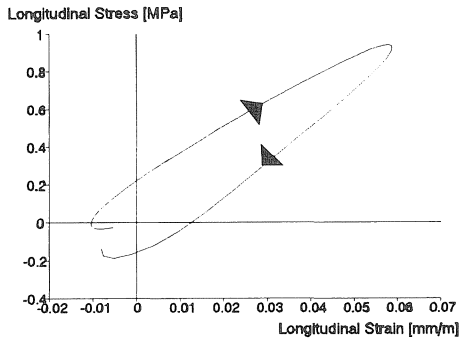


*Fig. 9a. Longitudinal stresses and strains in a Lissajou-plot.*

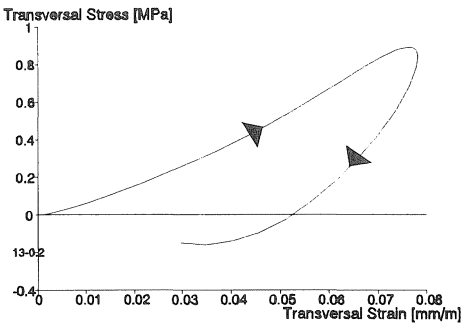


*Fig. 9b. Transversal stresses and strains in a Lissajou-plot.*

In Figure 10 the dissipated energy versus transversal distance is shown for several depths. Most energy is dissipated in the lower part of the upper layer. Of course the material properties are important here. Still, further analysis has shown that in the upper layer the energy is dissipated by shear components of the stresses and strains (in Cartesian coordinates), while in the second layer the orthogonal components cause are dominant.

## 8 Remarks and conclusion

Use of a linear visco-elastic material model enables new analysis of pavements. The asymmetric shape in strains, measured in full scale trials, can be backcalculated using material characteristics obtained in the laboratory. Ongoing studies have shown that extra information can be obtained on the behaviour of the (unbound) (sub)base. Especially in case a thin asphaltic layer is applied, modelling the unbound material elastically is insufficient. More details about this are given elsewhere (Nilsson et al. 1996).
From comparison of the width of the measured and calculated longitudinal and transversal strain curves one might also be able to determine the shape of the contact area of the tyre.
Permanent deformation can be analyzed in a principally correct way also. This should be especially of interest for engineers that face large deformation problems and want to know

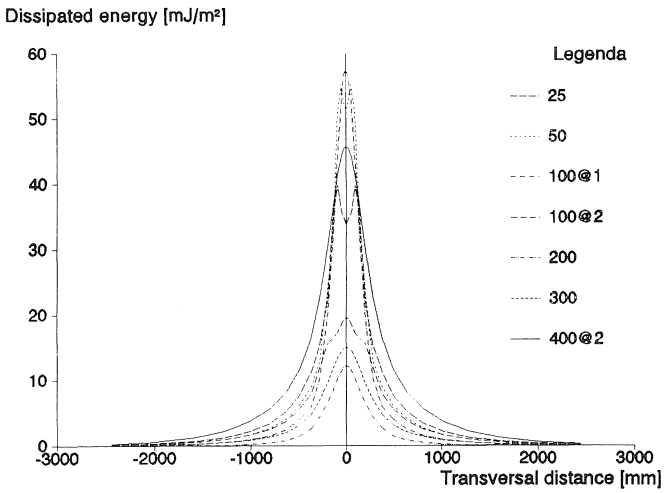


*Fig. 10. Dissipated energies versus transversal distance for several depths. The approriate layer is indicated.*

at what depth this deformation occurs, in equation to the traffic and their wheelconfiguration. Moreover dissipated energies due to a passage of a single wheel or of any set of wheels can be calculated. If dissipated energy is taken as a measure for damage initiation or development, the existing models for designing pavements change. One should consider other constructions and or

materials. The dissipated energy is not necessarily maximum at the bottom of the asphaltic layer: the maximum might well be at a locus high in the construction. This might yield an explanation for the development of surface cracks (cracks which are initiated at the surface and grow downwards).

If in road design full account is given to the visco-elastic properties of asphaltic concrete, the stress/strain distribution changes with respect to an elastic approach. Considering this point further leads to another detailed understanding of failures and thus to alternative pavement designs. Finally it is remarked that the VEROAD program might be helpful in calculating the amount of damage that various sets of wheels bring to the pavements.

## 9 Acknowledgement

The program VEROAD is has been developed under contract with the Road and Hydraulic Engineering Division of Rijkswaterstaat. The author acknowledges their permission to publish parts of the results. He acknowledges Dr. Frans van Cauwelaert cordially for his suggestions to overcome difficult phases in the study. Ir. Adrian Pronk is acknowledged for his enthusiasm and willingness to discuss the everyday progress of the project.

## 10 References

BATTIATO, G. and G. RONCA and C. VERGA. Moving Loads on a Visco-Elastic Double Layer: Prediction of Recoverable and Permanent Deformation. *Proceedings of the 4th International Conference on Structural Design of Asphalt Pavements*, Ann Arbor 1977.

BJÖRKLUND, A. *Creep Induced Behaviour of Resurfaced Pavements*. VTI-rapport, Nr. 271A 1984, ISSN 0347-6030.

BURMISTER D.M. The General Theory of Stresses and Displacements in Layered Soil Systems (I & II). *Journal of Applied Physics*, Volume 16, February & March, 1945.

CAUWELAERT VAN, F. Contraintes et Déplacements Dans un Massif Semi-Infini Isotrope ou à Isotropie Transverse Soumis à des Charges Rectangulaires Souples et Rigides en Surface. *Revue Francaise de Geotechnique*, No. 28, 1988.

CAUWELAERT VAN, F. *Bessel and Other Integral Transforms in Civil Engineering*. TU-Delft, ISSN 7-92-411-2, 1992.

FERRY, J.D. *Visco-Elastic Properties of Polymers*. Wiley, New York, 3rd edition, 1980.

GROENENDIJK, J. and C.H. VOGELZANG and A.A.A. MOLENAAR and L.J.J. DOHMEN. Performance tests under accelerated loadings with the LINTRACK test facility in the Netherlands. *4th Int. Conf. Bearing Capacity of Roads and Airfields*, Minneapolis 1994.

HOPMAN P.C. *Exploration of Different Methods to Calculate Dsas* and *Principles and first set up of computer code*; Report TUD,ISSN-0169-9288, No. 7-90-500-2, No. 7-90-500-12, No. 7-91-500-3 (in Dutch).

HOPMAN, P.C. *VEROAD: a Linear Visco-Elastic Multilayer Program for the Calculation of Stresses, Strains and Displacements in Asphaltic Road Constructions: A Visco-Elastic Halfspace*. Delft University of Technology, ISSN-0169-9288/7-93-500-6, 1993.

HOPMAN, P.C. *VEROAD: a Linear Visco-Elastic Multilayer Program For The Calculation of Stresses, Strains and Displacements in Asphaltic Road Constructions: A Visco-Elastic Multilayer System*. Delft University of Technology, ISSN-0169-9288/7-94-500-7, 1994.

HUANG, Y.H. Stresses and Displacements in Visco-Elastic Layered Systems Under Circular Loaded Areas. *Proceedings of the 2nd International Conference on Asphalt Pavements*, Ann Arbor 1967.

HUHTALA, M. The Rheology of Bituminous Binders. *First European Workshop: The Rheology of Binders*, April 1995.

ISHIHARA, K. The General Theory of Stresses and Displacements in Two-Layer Visco Elastic Systems. *Soil and Foundation*, Vol. 2 (1962).

JONG DE L. and M.G.F. PEUTZ and A.R. KORSWAGEN. *Computer Program BISAR, Layered Systems Under Normal and Tangential Surface Loads*; Koninklijke/Shell- Laboratorium, Amsterdam, AMSR.00006.73 Shell Research B.V., 1979.

NILSSON, R. and I. OOST and P.C. HOPMAN. Visco-Elastic Analysis of Full Scale Pavements: Validation of VEROAD. *Transport Research Board*, 1996.

TIMOSHENKO, S.P. and J.N. GOODIER. *Theory of Elasticity*. McGraw-Hill, 1970.

PAGEN, C.A. Dynamic Structural Properties of Asphalt Pavement Mixtures. *Proceedings of the 2nd International Conference on Asphalt Pavements*, Ann Arbor 1967.

PERLOFF, W.H. and F. MOAVENZADEH. Deflection of Visco-Elastic Medium Due to a Moving Load. *Proceedings of the 2nd International Conference on Asphalt Pavements*, Ann Arbor 1967.